Article (refereed) - postprint

Jarvie, Helen P.; Sharpley, Andrew N.; Kresse, Timothy; Hays, Phillip D.; Williams, Richard J.; King, Stephen M.; Berry, Lawrence G. 2018. **Coupling high-frequency stream metabolism and nutrient monitoring to explore biogeochemical controls on downstream nitrate delivery**. *Environmental Science & Technology*, 52 (23). 13708-13717.
https://doi.org/10.1021/acs.est.8b03074

Coupling high-frequency stream metabolism and nutrient monitoring to explore biogeochemical controls on downstream nitrate delivery

Helen P. Jarvie[1*], Andrew N. Sharpley[2], Timothy Kresse[3], Phillip D. Hays[4], Richard J. Williams[1], Stephen M. King[5], Lawrence G. Berry[2]

[1]*NERC Centre for Ecology and Hydrology, Wallingford, OX10 8BB, UK.*

[2]*Department of Crop Soil and Environmental Sciences, University of Arkansas, Fayetteville AR 72701, U.S.A.*

[3] *U.S. Geological Survey, Lower Mississippi-Gulf Water Science Center, 401 Hardin Rd., Little Rock, AR 72211, U.S.A.*

[4]*U.S. Geological Survey, Lower Mississippi-Gulf Water Science Center/University of Arkansas, Dept. of Geosciences, 216 Gearhart Hall, Fayetteville, AR 72701, U.S.A.*

[5]*STFC Rutherford Appleton Laboratory, Harwell Campus, Didcot, Oxfordshire, OX11 0QX, U.K.*

*corresponding author (hpj@ceh.ac.uk)

Key words: Nitrate, retention, stream, assimilation, denitrification, eutrophication, photosynthesis, respiration.

Abstract

Instream biogeochemical process measurements are often short term and localised. Here we use *in-situ* sensors to quantify the net effects of biogeochemical processes on seasonal patterns in baseflow nitrate retention at the river-reach scale. Dual-station high-frequency *in-situ* nitrate measurements, were coupled with high-frequency measurements of stream metabolism and dissolved inorganic carbon, in a tributary of the Buffalo National River, Arkansas. Nitrate assimilation was calculated from net primary production, and combined with mass-balance measurements, to estimate net nitrification and denitrification. The combined net effects of these instream processes (assimilation, denitrification and nitrification) removed >30-90% of the baseflow nitrate load along a 6.5km reach. Assimilation of nitrate by photoautotrophs during spring and early summer was buffered by net nitrification. Net nitrification peaked during the spring. After mid-summer, there was a pronounced switch from assimilatory nitrate uptake to denitrification. There was clear synchronicity between the switch from nitrate assimilation to denitrification, a reduction in river baseflows, and a shift in stream metabolism from autotrophy to heterotrophy. The results show how instream nitrate retention and downstream delivery is driven by seasonal shifts in metabolic pathways; and how continuous *in-situ* stream sensor networks offer new opportunities for quantifying the role of stream biota in the dynamics, fate, and transport of nitrogen in fluvial systems.

1. Introduction

Nutrients, including nitrogen (N), phosphorus (P), and carbon (C) from agriculture and domestic wastewater, are a major source of water-quality impairment[1]. Excessive nutrient inputs to rivers, streams, and lakes can accelerate growth of nuisance and harmful algae. Resulting increases in microbial activity and depletion of dissolved oxygen (DO) have profound negative consequences for invertebrates and fish, potable water supply, and recreation[2,3]. However, biogeochemical processes in streams also play an important role in regulating downstream nutrient transport, with stream biota retaining and removing nutrients from the water column, reducing downstream ecological impacts[4-6].

Streams can provide a major sink for nitrate (NO_3^-) through uptake (assimilation) by primary production and through denitrification[7,8]. The effectiveness of these processes varies throughout the year and between streams, but conventional methods for estimating NO_3^- uptake are based on relatively few, short-term experimental nutrient additions and isotope measurements[9-11], making results difficult to extrapolate in space and time[12]. Continuous high-frequency *in-situ* measurements offer new opportunities to explore NO_3^- source dynamics[13-17], and instream processes have been inferred from single-station diurnal concentration cycles[12,18,19], longitudinal profiling[20-23], and nested sensor networks[24].

In this study, we used *in-situ* sensors to quantify the net effects of biogeochemical processes on seasonal patterns in baseflow NO_3^- retention at the river-reach scale. The approach employed here is novel because it combines dual-station high-frequency NO_3^- measurements, with high-frequency measurements of stream metabolism (analysis of diurnal DO curves to calculate

primary production and respiration), dissolved inorganic carbon (DIC), and excess partial pressure of carbon dioxide ($EpCO_2$), to explore the capacity of instream biogeochemical processes to retain and remove NO_3^-. High-frequency *in-situ* monitoring of water chemistry and stream flow was undertaken along an experimental reach of Big Creek, a tributary of the Buffalo National Scenic River, Arkansas, U.S.A, and were used to calculate a NO_3^- mass balance along the reach. Net primary production was used to calculate NO_3^- assimilation by photoautotrophs. Daily NO_3^- removal rates and rates of NO_3^- assimilation by photoautotrophs were used to calculate net nitrification and denitrification. The biogeochemical controls on NO_3^- removal were then evaluated in relation to wider ecosystem drivers including streamflow, DO, and stream ecological function, to explore how seasonal shifts in metabolic pathways influence instream NO_3^- retention and downstream NO_3^- delivery.

2. Materials and Methods:

2.1 Site description and water-quality monitoring

Big Creek, a tributary of the Buffalo National Scenic River, Arkansas (Figure 1), is the subject of detailed water-quality monitoring because of a permitted swine concentrated animal feeding operation (CAFO) within the watershed, in operation since September 2013. The Big Creek watershed lies in the karst terrain of the Ozark Plateau of mid-continental USA (Figure 1). The watershed area is 236 km^2, with 79% of the land area deciduous forest, 3% evergreen forest, 14% grassland/pasture, and 3% developed land (see Supporting Information, S1.1). Swine-manure slurry from the CAFO has been land applied to permitted fields since January 1, 2014, in accordance with State regulations.

The focus of this study is an experimental reach of Big Creek, downstream of the CAFO, from an upstream monitoring station at Mt Judea (USGS site 07055790; watershed area 106 km^2) to a downstream monitoring station at Carver (USGS site 07055814; watershed area 233 km^2), 7.21 and 0.69 km from the confluence between Big Creek and the Buffalo River, respectively (Figure 1). One tributary (Left Fork) enters Big Creek between Mt Judea and Carver. The watershed is a mantled karst terrain characterized by intimate connection between groundwater and surface water; transport of surface-derived nutrients can be rapid[25] (see S1.2).

USGS conducted high-frequency (15-minute) NO_3^- monitoring using submersible ultraviolet nitrate probes at Carver (06/03/2014 to 04/29/2017) and Mt Judea (11/01/2014 to 11/01/2015); there was therefore one year of overlapping data (11/01/2014 to 11/01/2015), during which NO_3^- monitoring was undertaken at both Mt Judea and Carver. A water-quality sonde (YSI 6600) operating at Carver simultaneously collected 15-minute interval DO, pH, specific conductance, and water temperature data. Further information about the high-frequency water-quality monitoring is provided in S1.3.

Water-quality samples, collected on a weekly basis since 09/12/2013, with additional opportunistic high-flow sampling, at Mt Judea, Left Fork and at a groundwater (spring) monitoring site (Figure 1), provided NO_3^- (by ion chromatography, Dionex ICS-1600); alkalinity (by fixed-endpoint acidimetric titration to pH 4.5[26]); and conductivity (VWR Symphony B10C) data. Water quality data are available at https://bigcreekresearch.org/.

2.2 Stream-flow measurements and hydrograph separation

Stream flow was measured using established USGS streamflow gauging methods[27] (see S1.4). A two-component mixing model was used to partition the contributions to streamflow from groundwater and surface runoff[28], using alkalinity as a conservative groundwater tracer (see S1.5).

2.3 Analysis of diurnal dissolved oxygen curves to calculate primary production and respiration

The daily average gross primary production, daily average ecosystem respiration and reaeration coefficient were calculated from the series of diurnal DO curves at Carver, using a piecewise solution of the mass balance, DO model[29] simplified for the situation where the deficit does not vary spatially (Eq. 1): the Delta method[30,31].

$$dD/dt + k_a D = ER_{av} - GPP_{av}(t) \quad (1)$$

where D is the DO deficit (mg-O_2 L^{-1}), t is the time (days), k_a is the reaeration coefficient, ER_{av} is the ecosystem respiration (mg-O_2 L^{-1} d^{-1}), and GPP_{av} is the gross primary production (mg-O_2 L^{-1} d^{-1}); these are standard measures of ecosystem respiration and gross primary production in river systems[32].

Odum[33] suggested a classification system of flowing-water communities based on oxygen metabolism by using the ratio of GPP_{av} to ER_{av} (*GPP/ER*). Respiration is associated with both plant and microbial activity. Photosynthesis is only associated with plants. Autotroph-dominated communities are represented by *GPP/ER* values > 1, whereas heterotroph-dominated communities are represented by *GPP/ER* values < 1.

2.5 Use of the THINCARB model for calculating dissolved inorganic carbon concentrations and excess partial pressure of carbon dioxide

The THINCARB model (THermodynamic modelling of INorganic CARBon)[34] uses pH, Gran Alkalinity (Alk_{Gran}) and temperature measurements to calculate dissolved inorganic carbon (DIC) concentrations and DIC speciation from the excess partial pressures of carbon dioxide ($EpCO_2$) in freshwaters. THINCARB is open access and is described in detail in Jarvie et al (2017)[34]; an outline is provided in SI1.8. Prior to use, alkalinity measurements in units of mg-$CaCO_3$ L^{-1} were first converted to Alk_{Gran} (in µeq L^{-1}), where 1 mg L^{-1} $CaCO_3$ = 19.98 µeq L^{-1} [34].

THINCARB was applied to the high-frequency sonde data from Carver. Specific conductance was used as a surrogate for alkalinity: using the regression relationship between Alk_{Gran} and specific conductance (κ), measured across the Big Creek watershed, including the spring, and Mt Judea, Left Fork and Carver stream sites: Alk_{Gran} = 8.65 (±0.28) × κ – 6.44 (±66), R^2 = 0.95, n=270, P<0.001 (numbers in parentheses represent twice the standard error). By applying this regression equation to the hourly κ series, an hourly alkalinity record was derived, which was then used alongside the hourly pH and water-temperature data, to calculate a high-frequency DIC and $EpCO_2$ series.

2.6 Mass-balance calculation of baseflow nitrate fluxes, instream losses and net nitrification and denitrification

Daily mass-balance calculations were undertaken for eight quiescent, low-flow periods (each typically of 1-2 weeks). USGS stream-velocity readings from Carver ranged from 0.457 and 1.22 m s^{-1}, and with a stream distance of 6.38 km, the travel times ranged from 3.87 h to 1.45 h.

148 Therefore, daily mass balances over a 24-h period were assumed sufficient to account for
149 transit of NO_3^-, given: (a) the relatively short travel times; (b) the high degree of stationarity in
150 flux transfers during quiescent baseflow conditions; and (c) that calculated daily mass balances
151 were averaged over a 1-2 week period.

152 The 15-minute NO_3^- measurements at Mt Judea and Carver were converted to daily means, and
153 daily nitrate loads at each site were calculated using the corresponding gauged daily stream-
154 flow data. To account for flow accretion along the reach, the difference between the daily flow
155 downstream at Carver and the upstream site at Mt Judea was calculated. The increase in flows
156 was assumed to be input from Left Fork (Figure 1).

157 Daily NO_3^- input loading to the reach (L_T) was calculated as the sum of the daily NO_3^- loads from
158 Mt Judea (L_{MJ}) and Left Fork (L_{LF}):

159 $$L_T = L_{MJ} + L_{LF} \quad (2)$$

160 There was no high-resolution NO_3^- monitoring on Left Fork, so weekly NO_3^- measurements from
161 grab samples taken at Left Fork were combined with the measured daily flow accretion to
162 derive daily loads from Left Fork (S1.6.1). A sensitivity analysis evaluated the potential effects of
163 under- or over-estimating Left Fork NO_3^- concentrations by ±50% (Tables SI1 and SI2).

164 Within this karst watershed, some of the flow accretion will arise from direct groundwater
165 input into Big Creek. Discharge data were not available from the Left Fork tributary, and direct
166 apportionment of contributions from Left Fork and groundwater was not possible. We
167 therefore evaluated a second, alternative 'endmember' case scenario whereby all of flow
168 accretion was attributed to direct groundwater contribution (S1.6.2).

The daily instream NO_3^- load removal (L_R) along the reach was calculated as the difference between the daily input NO_3^- loading (L_T), and the daily NO_3^- load at Carver (L_C):

$$L_R = L_T - L_C \quad (3)$$

To allow direct comparison with rates of assimilatory NO_3^- uptake by photosynthesis, L_R (kg-N d^{-1}) was then converted to a daily NO_3^- removal rate, U_T (mg-N L^{-1} d^{-1}). U_T incorporates both assimilatory NO_3^- uptake by photoautotrophs (U_A), heterotrophic NO_3^- removal through direct uptake and denitrification (U_D), and NO_3^- enrichment due to remineralization via nitrification (R)[20]:

$$U_T = U_A + U_D - R \quad (4)$$

U_A was estimated from the GPP_{av} measurements[12,35]. GPP_{av} data were converted into net primary production (*NPP*), assuming that autotrophic respiration consumed 50% of the GPP_{av}[36,37]. NPP data were then converted from units of O_2 uptake (mg-O_2 L^{-1} d^{-1}) to C uptake (mg-C L^{-1} d^{-1}), with a photosynthetic quotient of 1.00, then converted to NO_3^- uptake (mg-N L^{-1} d^{-1}), using a molar ratio of C:N of 12[38]. Subtracting U_T from U_A provides a measure of either net nitrification (positive values) or net heterotrophic NO_3^- removal through direct uptake and denitrification, hereafter referred to as 'net denitrification' (negative values). When the river was influent, loss of NO_3^- to groundwater was accounted for, as described in S1.6.3.

3. Results and Discussion

3.1 Three-year time series of nitrate, dissolved inorganic carbon and stream metabolism

188 The hourly NO_3^- and DIC concentrations variations at Carver were driven by streamflow, but in
189 opposing directions (Figure 2a). The mean and median NO_3^- concentrations were 0.128 and
190 0.093 mg-N L^{-1}, respectively. Nitrate concentrations at Carver were lowest during baseflow
191 (mean 0.043 mg-N L^{-1}; lowest 10% of flows) and highest during storm runoff (mean 0.278 mg-N
192 L^{-1}; highest 10% of flows), arising from nonpoint-source mobilisation and delivery of NO_3^- from
193 watershed soils during rainfall events.

194 The mean and median DIC concentrations were 24.8 and 25.2 mg-C L^{-1}, respectively. DIC
195 concentrations were highest during baseflow (mean 31.7 mg-C L^{-1}), with DIC concentrations
196 diluted by storm runoff (mean 13.2 mg-C L^{-1}). Highest DIC and lowest NO_3^- concentrations
197 occurred during the extended low-flows between August and November 2015.

198 The mean and median molar C:N ratios were 356 and 305, respectively. The mean C:N ratio
199 during baseflow was 882, and 82 during stormflow. C:N ratios greater than ~6.6 are indicative
200 of stoichiometric depletion of N relative to C[39]. Absolute NO_3^- concentrations below ~0.1 mg-N
201 L^{-1} are deemed likely to be limiting to algae, with algal growth response to NO_3^- enrichment
202 occurring between 0.38 to 1.79 mg-N L^{-1} [40]. Therefore, under average and baseflow conditions
203 at Carver, a clear potential exists for algal growth to be limited by low NO_3^- availability.

204 No longer-term trends in either NO_3^- or DIC were observed over the three years. These high-
205 frequency monitoring results are consistent with results from near-weekly water quality
206 monitoring of Big Creek at Mt Judea, which showed no statistically significant increasing or
207 decreasing trends in dissolved or particulate forms of P and N concentrations since 2013[41].

Earlier studies[6] have shown that Ozark streams can be very effective at retaining available nutrients, and buffering additional nutrient inputs. Therefore, the absence of any increasing trend in nutrients in the water column may result from the rapid and efficient uptake of nutrient inputs by stream biota. Consequently, high-resolution stream metabolism and nutrient measurements were used here to detect whether increased photosynthesis or respiration rates resulted from increased nutrient assimilation, even where no increases in water-column nutrient concentrations could be observed.

The time series in daily rates of GPP_{av} and ER_{av}, at Carver (Figure 2b), showed no definitive long-term trends between 2014 and 2017. GPP_{av} declined rapidly in response to major storm runoff events, but typically recovered within a couple of weeks. Highest GPP_{av} tended to occur during quiescent baseflow or recessional streamflow conditions during the summer (May through August). Both GPP_{av} and ER_{av} declined during the autumn (September through December), reflecting reductions in stream biological activity, and GPP_{av} tended to decline at a faster rate than *ER*. This was particularly apparent during the extended low-flows between August and December 2015, suggesting a decline in primary production relative to microbial activity and a transition from net autotrophic to net heterotrophic stream communities. During winter baseflows (November through January), ER_{av} tended to exceed GPP_{av}. During the 3-yr monitoring, no CAFO-related impacts on either stream nutrient concentrations or metabolism are discernible at Carver.

3.2 Temporal and spatial variability in NO_3^- concentrations, relative to other key environmental variables

Mean daily NO_3^- concentrations varied between baseflow and storm events at Mt Judea and Carver, during the one year of overlapping data (Figure 3). There was a clear differentiation between a higher-flow period characterised by regular storm events from mid-December 2014 to mid-July 2015, and lower-flow conditions from August to November/December 2015 (Figures 3 and 4).

During the higher-flow period, a positive correlation existed between upstream (Mt Judea) and downstream (Carver) NO_3^-, with a ratio approaching 1 (Figure 3). During this high-flow period, NO_3^- concentrations at both upstream and downstream sites ranged between ~0.1 and ~0.4 mg-N L^{-1}. Time series data show close convergence between upstream and downstream NO_3^- concentrations during storm-event peak concentrations (Figure 4a,b).

Under lower-flow conditions, NO_3^- concentrations were consistently higher upstream than downstream (Figure 3). The increase in NO_3^- concentrations at the upstream site during the summer and autumn 2015 corresponds with reductions in flow. This is typical of the longer-term hydrologically-driven cycles in NO_3^- concentrations observed at the upstream site, reflecting a strong flow dependency, with highest concentrations under the lowest flows, and dilution with increasing flow (Figure SI1). The strong increase in NO_3^- concentrations during July to November 2015 therefore reflects hydrological controls, and is consistent with falling flows. The high NO_3^- concentrations in autumn 2015 subsequently declined with the onset of higher flows (Fig SI1a,b).

The gap in NO_3^- concentrations between upstream and downstream sites widened with decreasing flow, particularly during the protracted low-flows between mid-July and November

2015. During this time, minimal soil water contributed to streamflow, and almost all (>95%) of streamflow was derived from ground water (Figure 4a,b). By the end of October 2015, upstream NO_3^- concentrations reached ~0.75 mg-N L^{-1}, whereas downstream NO_3^- concentrations were ~0.05 mg-N L^{-1}. Between July and November 2015, downstream NO_3^- concentrations exhibited a much lower range (~0.05 to ~0.15 mg-N L^{-1}) as compared with upstream (~0.1 to ~0.8 mg-N L^{-1}) (Figure 3). This reduction in both magnitude and range of downstream NO_3^- concentrations under baseflow conditions could arise either from dilution of NO_3^-, as a result of downstream accretion of water sources with much lower NO_3^- concentrations, or by removal of NO_3^- through biogeochemical processes, necessitating a mass-balance evaluation (see section 3.3).

The widening gap in NO_3^- concentrations between upstream and downstream sites after mid-July 2015 corresponded with a decline in *GPP/ER*, which fell below 1, indicating a change to net heterotrophy (Figure 4c). During the low-flow period from mid-July to November 2015, Big Creek was heterotrophic for ~90% of days. Daily streamwater $EpCO_2$ doubled between mid-July and November 2015, from 4.5 to 9.1 times atmospheric pressure, independently confirming an increase in rates of respiration (CO_2 release), relative to photosynthesis (CO_2 uptake).

During the higher-flow period from mid-January to mid-July, Big Creek was predominantly net autotrophic (*GPP/ER* >1 for 52% of days). Net heterotrophic conditions prevailed predominantly during lower-flow intervals between storm events, with *GPP/ER* <1 typically during and immediately-after storm events.

Molar C:N ratios at Carver also increased markedly after mid-July, from ~300 to >800 (Figure 4d). This stoichiometric depletion of N, along with persistence of low NO_3^- concentrations below 0.1 mg-N L^{-1} (falling to <0.04 mg-N L^{-1}), suggests that algal growth may have been limited by low N availability at Carver over the late summer and autumn of 2015.

3.3 Nitrate reach mass balance to quantify seasonal nitrate removal during baseflow conditions

Mean daily NO_3^- mass balances for the eight seasonal quiescent baseflow periods between February and October 2015 are presented in Table 1. Mean daily NO_3^- input loadings to the reach (L_T) increased from 17.3 kg-N d^{-1} in February to 61.7 kg-N d^{-1} in July, then declined rapidly to 7.56 kg-N d^{-1} in August, which also corresponded with an order of magnitude reduction in baseflow discharge. By October, L_T had fallen to only 2.98 kg-N d^{-1}. Instream NO_3^- removal (L_R) followed a similar pattern to L_T, with highest mean daily instream NO_3^- removal during June (24 kg-N d^{-1}), then decreasing during the late summer and autumn, and falling to 2.82 kg-N d^{-1} in October. However, the efficiency of instream NO_3^- removal (U_E, i.e., L_R expressed as a percentage of L_T) increased markedly during the late summer and autumn, from 32% in July to 74-95% between August and October.

The fluvial mass balance therefore confirmed that the observed downstream reductions in NO_3^- concentrations under baseflow were a result of net instream removal of NO_3^- by biogeochemical processes, rather than a dilution effect.

Although L_T and L_R were greatest during the winter to early summer period, U_E and the instream NO_3^- removal rate (U_T) increased dramatically during the low flows of the late summer and autumn; U_T increased from ≤0.09 mg-N L^{-1} d^{-1} (February through July), to >0.2 mg-N L^{-1} d^{-1} in

August and September, and 0.66 mg-N L^{-1} d^{-1} in October (Table 2). By autumn 2015, >75% of the NO_3^- inputs were removed by biogeochemical processes (Table 1).

We also assessed the efficiency of NO_3^- removal under the alternative scenario, where the increase in flow along the experimental reach was solely from direct groundwater input (S1.6.2). This made relatively little difference to the U_E, which also increased markedly during the late summer and autumn, from 46% in July to 72-94% between August and October (Table SI3). The sensitivity analysis (Tables SI1 and SI3) showed that a 50% increase or decrease in either Left Fork or groundwater NO_3^- concentrations made little difference to these findings: a consistent increase in efficiency of NO_3^- removal was observed after July, with August to October U_E values consistently ~70-95%.

3.4 Biogeochemical controls on nitrate delivery: accounting for assimilatory nitrate uptake to calculate net nitrification and net denitrification

From February to July, assimilatory NO_3^- uptake by photosynthesising plants (U_A) consistently exceeded U_T (Table 2) indicating, firstly, that assimilation of NO_3^- by photoautotrophs was the dominant process removing NO_3^- from the water column; and secondly that assimilation was partially balanced by net nitrification NO_3^- gains. In contrast, from August to October, U_T exceeded U_A, indicating that heterotrophic NO_3^- removal through direct uptake and denitrification was removing NO_3^- along the reach in late summer and autumn.

Table 3 shows that net nitrification gains to the reach ranged from 0.135 mg-N L^{-1} d^{-1} in February to 0.273 mg-N L^{-1} d^{-1} in April/May. However, after July, a pronounced switch from net nitrification gains to net denitrification losses occurred. During late summer and autumn, denitrification

312 losses of NO_3^- increased from ~0.100 mg-N L^{-1} d^{-1} in August and September to 0.592 mg-N L^{-1} d^{-1}
313 in October. These estimates were based on using an average periphyton C:N molar ratio of 12
314 for U.S.A. streams[35,38]. We also evaluated the effects of using an average periphyton molar C:N
315 ratio of 8.6, from research in northern European streams[17]. This increased U_A values by ~39%,
316 but did not alter our findings of a switch between net nitrification between February and July, to
317 net denitrification from August to October. By changing the C:N stoichiometry from 12 to 8.6,
318 net nitrification ranged from +0.218 mg-N L^{-1} d^{-1} in February to +0.414 mg-N L^{-1} d^{-1} in April/May,
319 with net denitrification ranging from -0.033 mg-N L^{-1} d^{-1} in August to -0.562 mg-N L^{-1} d^{-1} in
320 October.

321 Net nitrification and denitrification rates were compared with mean daily *GPP/ER*, $EpCO_2$,
322 streamflow and percentage groundwater discharge (Table 3). The shift from net nitrification to
323 net denitrification corresponded directly with: (1) a change in stream metabolism from net
324 autotrophic (*GPP/ER* in July was 1.97) to net heterotrophic (*GPP/ER* fell below 1, to 0.78 in
325 August, 0.62 in September, and 0.57 in October); and (2) an increase in $EpCO_2$ and a reduction
326 in DO arising from the increases in microbial respiration relative to photosynthesis.

327 The alternative scenario where flow accretion between Mt Judea and Carver was attributed to
328 direct groundwater discharge to Big Creek also had no effect on the timing of the shift from net
329 nitrification to denitrification (S1.6.2, Table SI4). Sensitivity analysis (Tables SI2 and SI4) also
330 showed that, irrespective of a 50% increase or decrease in either Left Fork or groundwater NO_3^-
331 concentrations, the same consistent switch between net nitrification and net denitrification
332 was observed after July.

The consistency in this observed switch between instream NO_3^- production and instream NO_3^- removal, and its synchronicity with measured changes in stream metabolism, provides compelling evidence that the marked change in instream NO_3^- processing and delivery after July was linked to changes in stream metabolism from net autotrophy to net heterotrophy.

The karst streams of the Ozarks are characterised by a large hyporheic zone[42,43], a hotspot of nitrogen transformation[44]. Water residence times and redox conditions provide a key control on changes between NO_3^- removal and NO_3^- production with hyporheic zone sediments[45-48]. In Big Creek, the winter to mid-summer period was characterised by higher baseflows (at least an order of magnitude greater than late summer/autumn baseflows), and net autotrophy resulting in higher instream DO concentrations. Rapid movement of well-oxygenated water throughout the water column, and into the hyporheic zone, promotes aerobic metabolism of organic matter and release of NO_3^- through nitrification[46,49]. From winter to mid-summer, net nitrification was observed in Big Creek, and nitrification in the hyporheic zone may have been responsible for buffering the effects of photosynthetic assimilatory uptake of NO_3^-.

Under the more sluggish flow conditions during late summer and autumn, available oxygen is depleted as a result of increased heterotrophic activity. The reduced movement of water and oxygen through the hyporheic zone favors a shift in respiratory pathways with denitrification (conversion of nitrate to N_2O and/or N_2 gas)[50,51]. Unlike assimilation of NO_3^- into plant biomass, which retains N temporarily, denitrification results in a permanent loss of bioavailable N. The low baseflows of late summer and autumn 2015, resulted in higher water residence times and a greater proportion of flow moving through the hyporheic zone. This provides greater exposure and water contact time with microbial biofilms where denitrification occurs[51]. The death and

355 breakdown of biomass during the late summer and autumn contribute to the availability of
356 organic matter for microbial decomposition, promoting higher rates of microbial respiration
357 relative to photosynthesis, losses of DO, and greater availability of organic carbon as a resource
358 for denitrifying bacteria[45,53]. Denitrification within the hyporheic zone may therefore be
359 responsible for losses of NO_3^- in Big Creek during the late summer and autumn. Although
360 denitrification can also occur on suspended sediments within the water column[54,55], this is likely
361 to be a second order effect under baseflow conditions in a groundwater-fed stream, where
362 suspended solids concentrations are low (typically <5 mg L^{-1}).

363 Under baseflow conditions, instream assimilatory NO_3^- uptake by photosynthesising plants and
364 hyporheic-zone denitrification along the experimental reach removed between ~30 and ~90%
365 of the NO_3^- input load. During the period of monitoring (spring 2014 to spring 2017) NO_3^-
366 loading to the upstream section of Big Creek (at Mt Judea) was attenuated by instream
367 processing such that no CAFO-related impacts on either stream nutrient concentrations or
368 metabolism were discernible at the downstream location (Carver), and thus, to the Buffalo
369 River. Future monitoring will be needed to detect whether long-term changes in nutrients and
370 organic carbon inputs may occur, whether this stimulates higher rates of heterotrophic and/or
371 autotrophic activity, and any longer-term effects on the capacity of assimilation and
372 denitrification processes to remove and buffer any increase in nutrient loadings.

373 The novelty of this research is the combination of continuous, high-frequency *in-situ* stream
374 metabolism and nitrate measurements, to apportion the net effects of assimilation,
375 nitrification, and denitrification on changes in baseflow nitrate fluxes at the river-reach to
376 watershed scale. In this case, we found that, during winter to mid-summer periods, NO_3^- uptake

in Big Creek was dominated by assimilation by photoautotrophs, which was partially compensated by release of NO_3^- from nitrification. In late summer, the predominant metabolic pathway switched to net heterotrophy and heterotrophic NO_3^- removal through direct uptake and denitrification became the dominant process of nitrate removal. Removal of NO_3^- by assimilation and denitrification provides an important "self-cleansing" ecosystem service, resulting in a pronounced shift in C:N stoichiometry and decreasing NO_3^- concentrations to low levels which would be expected to limit algal growth[56].

This approach provides a means scaling up, from micro-scale and meso-scale process experiments and measurements, which are, by necessity, short term and localised, to explore how river nitrate delivery responds to shifts in stream metabolism, from day-to-day and seasonal to inter-annual variability. This research, and the methods presented here, are applicable along the river continuum, from headwaters to large-scale fluvial systems (with large spatial and temporal variability in nutrient fluxes), and offer a valuable way forward in quantifying net process controls on the fate and transport of nitrogen in fluvial systems.

Acknowledgements:

HPJ and RJW were supported by NERC National Capability projects NEC05966 and NEC04879. Funding for the Big Creek Research and Extension monitoring was provided by the Arkansas Governor's Office and State Legislature to the University of Arkansas System's Division of Agriculture. Hydrological and chemical monitoring by the USGS were supported by a National Park Service/USGS Water Quality Partnership Grant, administered by the USGS.

Supporting Information (see accompanying PDF file)

- Number of pages: 16
- Number of Figures: 1
- Number of Tables: 4

List of Figures:

pressure of carbon dioxide ($EpCO_2$); (d) streamflow and the molar C:N ratio (dissolved organic carbon/NO_3-N).

List of Tables:

Table 1: Seasonal patterns in mean daily NO_3^- input loadings (L_T) to Big Creek, mean daily instream NO_3^- load removal (L_R) along the experimental reach, under low-flow conditions, and mean daily NO_3^- load removal as a percentage of NO_3^- inputs (U_E).

Table 2: Seasonal patterns in mean daily NO_3^- removal rate (U_T) along the experimental reach of Big Creek, under low-flow conditions, and mean daily assimilatory uptake of NO_3-N by photoautotrophs (U_A).

Table 3: Seasonal patterns in mean daily NO_3^- concentration gains by net nitrification and losses by net denitrification along the experimental reach of Big Creek, under low-flow conditions, with mean daily values of the ratio between gross primary production and ecosystem respiration (*GPP/ER*), excess partial pressure of carbon dioxide ($EpCO_2$), dissolved oxygen (DO), stream flow and the percentage of groundwater contribution to stream flow.

References

1. Smith, V. H., Eutrophication of freshwater and coastal marine ecosystems - A global problem. Environmental Science and Pollution Research **2003**, 10, (2), 126-139.

2. Dodds, W. K.; Bouska, W. W.; Eitzmann, J. L.; Pilger, T. J.; Pitts, K. L.; Riley, A. J.; Schloesser, J. T.; Thornbrugh, D. J., Eutrophication of US Freshwaters: Analysis of Potential Economic Damages. Environmental Science & Technology **2009**, 43, (1), 12-19.

3. Dodds, W. K.; Smith, V. H., Nitrogen, phosphorus, and eutrophication in streams. Inland Waters **2016**, 6, (2), 155-164.

4. Peterson, B. J.; Wollheim, W. M.; Mulholland, P. J.; Webster, J. R.; Meyer, J. L.; Tank, J. L.; Marti, E.; Bowden, W. B.; Valett, H. M.; Hershey, A. E.; McDowell, W. H.; Dodds, W. K.; Hamilton, S. K.; Gregory, S.; Morrall, D. D., Control of nitrogen export from watersheds by headwater streams. Science **2001**, 292, (5514), 86-90.

5. Alexander, R. B.; Boyer, E. W.; Smith, R. A.; Schwarz, G. E.; Moore, R. B., The role of headwater streams in downstream water quality. Journal of the American Water Resources Association **2007**, 43, (1), 41-59.

6. Jarvie, H. P.; Sharpley, A. N.; Scott, J. T.; Haggard, B. E.; Bowes, M. J.; Massey, L. B., Within-River Phosphorus Retention: Accounting for a Missing Piece in the Watershed Phosphorus Puzzle. Environmental Science & Technology **2012**, 46, (24), 13284-13292.

7. Mulholland, P. J.; Helton, A. M.; Poole, G. C.; Hall, R. O.; Hamilton, S. K.; Peterson, B. J.; Tank, J. L.; Ashkenas, L. R.; Cooper, L. W.; Dahm, C. N.; Dodds, W. K.; Findlay, S. E. G.; Gregory, S. V.; Grimm, N. B.; Johnson, S. L.; McDowell, W. H.; Meyer, J. L.; Valett, H. M.; Webster, J. R.; Arango, C. P.; Beaulieu, J. J.; Bernot, M. J.; Burgin, A. J.; Crenshaw, C. L.; Johnson, L. T.; Niederlehner, B. R.; O'Brien, J. M.; Potter, J. D.; Sheibley, R. W.; Sobota, D. J.; Thomas, S. M., Stream denitrification across biomes and its response to anthropogenic nitrate loading. Nature **2008**, 452, (7184), 202-U46.

8. Mulholland, P. J.; Valett, H. M.; Webster, J. R.; Thomas, S. A.; Cooper, L. W.; Hamilton, S. K.; Peterson, B. J., Stream denitrification and total nitrate uptake rates measured using a field N-15 tracer addition approach. Limnology and Oceanography **2004**, 49, (3), 809-820.

9. Tank, J. L.; Marti, E.; Riis, T.; von Schiller, D.; Reisinger, A. J.; Dodds, W. K.; Whiles, M. R.; Ashkenas, L. R.; Bowden, W. B.; Collins, S. M.; Crenshaw, C. L.; Crowl, T. A.; Griffiths, N. A.; Grimm, N. B.; Hamilton, S. K.; Johnson, S. L.; McDowell, W. H.; Norman, B. M.; Rosi, E. J.; Simon, K. S.; Thomas, S. A.; Webster, J. R., Partitioning assimilatory nitrogen uptake in streams: an analysis of stable isotope tracer additions across continents. Ecological Monographs **2018**, 88, (1), 120-138.

10. Tank, J. L.; Meyer, J. L.; Sanzone, D. M.; Mulholland, P. J.; Webster, J. R.; Peterson, B. J.; Wollheim, W. M.; Leonard, N. E., Analysis of nitrogen cycling in a forest stream during autumn using a N-15-tracer addition. Limnology and Oceanography **2000**, 45, (5), 1013-1029.

11. Ensign, S. H.; Doyle, M. W., Nutrient spiraling in streams and river networks. Journal of Geophysical Research-Biogeosciences **2006**, 111, (G4). G04009, doi:10.1029/2005JG000114.

12. Rode, M.; Halbedel Angelstein, S.; Anis, M. R.; Borchardt, D.; Weitere, M., Continuous in-stream assimilatory nitrate uptake from high frequency sensor measurements. Environmental Science & Technology **2016**, 50, (11), 5685-5694.

13. Bowes, M. J.; Jarvie, H. P.; Halliday, S. J.; Skeffington, R. A.; Wade, A. J.; Loewenthal, M.; Gozzard, E.; Newman, J. R.; Palmer-Felgate, E. J., Characterising phosphorus and nitrate inputs to a rural river using high-frequency concentration-flow relationships. Science of the Total Environment **2015**, 511, 608-620.

14. Halliday, S. J.; Skeffington, R. A.; Wade, A. J.; Bowes, M. J.; Gozzard, E.; Newman, J. R.; Loewenthal, M.; Palmer-Felgate, E. J.; Jarvie, H. P., High-frequency water quality monitoring in an urban catchment: hydrochemical dynamics, primary production and implications for the Water Framework Directive. Hydrological Processes **2015**, 29, (15), 3388-3407.

15. Halliday, S. J.; Skeffington, R. A.; Wade, A. J.; Bowes, M. J.; Read, D. S.; Jarvie, H. P.; Loewenthal, M., Riparian shading controls instream spring phytoplankton and benthic algal growth. Environmental Science-Processes & Impacts **2016**, 18, (6), 677-689.

16. Wade, A. J.; Palmer-Felgate, E. J.; Halliday, S. J.; Skeffington, R. A.; Loewenthal, M.; Jarvie, H. P.; Bowes, M. J.; Greenway, G. M.; Haswell, S. J.; Bell, I. M.; Joly, E.; Fallatah, A.; Neal, C.; Williams, R. J.; Gozzard, E.; Newman, J. R., Hydrochemical processes in lowland rivers: insights from in situ, high-resolution monitoring. Hydrology and Earth System Sciences **2012**, 16, (11), 4323-4342.

17. Rode, M.; Wade, A. J.; Cohen, M. J.; Hensley, R. T.; Bowes, M. J.; Kirchner, J. W.; Arhonditsis, G. B.; Jordan, P.; Kronvang, B.; Halliday, S. J.; Skeffington, R. A.; Rozemeijer, J. C.; Aubert, A. H.; Rinke, K.; Jomaa, S., Sensors in the stream: The High-frequency wave of the present. Environmental Science & Technology **2016**, 50, (19), 10297-10307.

18. Cohen, M. J.; Kurz, M. J.; Heffernan, J. B.; Martin, J. B.; Douglass, R. L.; Foster, C. R.; Thomas, R. G., Diel phosphorus variation and the stoichiometry of ecosystem metabolism in a large spring-fed river. Ecological Monographs **2013**, 83, (2), 155-176.

19. Hensley, R. T.; Cohen, M. J., On the emergence of diel solute signals in flowing waters. Water Resources Research **2016**, 52, (2), 759-772.

20. Hensley, R. T.; Cohen, M. J.; Korhnak, L. V., Inferring nitrogen removal in large rivers from high-resolution longitudinal profiling. Limnology and Oceanography **2014**, 59, (4), 1152-1170.

21. Kunz, J. V.; Hensley, R.; Brase, L.; Borchardt, D.; Rode, M., High frequency measurements of reach scale nitrogen uptake in a fourth order river with contrasting hydromorphology and variable water chemistry (Weisse Elster, Germany). Water Resources Research **2017**, 53, (1), 328-343.

22. Kraus, T. E. C.; O'Donnell, K.; Downing, B. D.; Burau, J. R.; Bergarnaschi, B. A., Using paired in situ high frequency nitrate measurements to better understand controls on nitrate concentrations and estimate nitrification rates in a wastewater-impacted river. Water Resources Research **2017**, 53, (10), 8423-8442.

23. Jones, C.; Kim, S. W.; Schilling, K., Use of continuous monitoring to assess stream nitrate flux and transformation patterns. Environmental Monitoring and Assessment **2017**, 189: 35; DOI 10.1007/s10661-016-5749-6.

24. Wollheim, W. M.; Mulukutla, G. K.; Cook, C.; Carey, R. O., Aquatic nitrate retention at river network scales across flow conditions determined using nested in situ sensors. Water Resources Research **2017**, 53, (11), 9740-9756.

25. Jarvie, H. P.; Sharpley, A. N.; Brahana, V.; Simmons, T.; Price, A.; Neal, C.; Lawlor, A. J.; Sleep, D.; Thacker, S.; Haggard, B. E., Phosphorus retention and remobilization along hydrological pathways in karst terrain. Environmental Science & Technology **2014**, 48, (9), 4860-4868.

26. American Public Health Association (APHA), Alkalinity: Titration Method 2320 B. In: Standard methods for the examination of water and wastewater. 23rd Edition **1987.** ISBN: 978-0-87553-287-5.

27. Rantz, S.E., Measurement and computation of streamflow: Volume 1, Measurement of stage and discharge. In U.S. Geological Survey, Water Supply Paper 2175. **1982**.

28. Jarvie, H. P.; Neal, C.; Smart, R.; Owen, R.; Fraser, D.; Forbes, I.; Wade, A., Use of continuous water quality records for hydrograph separation and to assess short-term variability and extremes in acidity and dissolved carbon dioxide for the River Dee, Scotland. Science of the Total Environment **2001**, 265, (1-3), 85-98.

29. O'Connor, D. J.; Ditoro, D. M., Photosynthesis and oxygen balance in streams. Journal of the Sanitary Engineering Division. Proceedings of the American Society of Civil Engineers **1970**, 96, (2), 547-571

30. Williams, R. J.; White, C.; Harrow, M. L.; Neal, C., Temporal and small-scale spatial variations of dissolved oxygen in the Rivers Thames, Pang and Kennet, UK. Science of the Total Environment **2000**, 251, 497-510.

31. Chapra, S. C.; Ditoro, D. M., Delta method for estimating primary production, respiration, and reaeration in streams. Journal of Environmental Engineering-ASCE **1991**, 117, (5), 640-655.

32. Bernhardt, E. S.; Heffernan, J. B.; Grimm, N. B.; Stanley, E. H.; Harvey, J. W.; Arroita, M.; Appling, A. P.; Cohen, M. J.; McDowell, W. H.; Hall, R. O.; Read, J. S.; Roberts, B. J.; Stets, E. G.; Yackulic, C. B., The metabolic regimes of flowing waters. Limnology and Oceanography 2018, 63, S99-S118.

33. Odum, H. T., Primary production in flowing waters. Limnology & Oceanography **1956**, 1, 102–117.

34. Jarvie, H. P.; King, S. M.; Neal, C., Inorganic carbon dominates total dissolved carbon concentrations and fluxes in British rivers: Application of the THINCARB model - Thermodynamic modelling of inorganic carbon in freshwaters. Science of the Total Environment **2017**, 575, 496-512.

35. King, S. A.; Heffernan, J. B.; Cohen, M. J., Nutrient flux, uptake, and autotrophic limitation in streams and rivers. Freshwater Science **2014**, 33, (1), 85-98.

36. Hall, R. O.; Tank, J. L., Ecosystem metabolism controls nitrogen uptake in streams in Grand Teton National Park, Wyoming. Limnology and Oceanography **2003**, 48, (3), 1120-1128.

37. Hall, R. O.; Beaulieu, J. J., Estimating autotrophic respiration in streams using daily metabolism data. Freshwater Science **2013**, 32, (2), 507-516.

38. Stelzer, R. S.; Lamberti, G. A., Effects of N : P ratio and total nutrient concentration on stream periphyton community structure, biomass, and elemental composition. Limnology and Oceanography **2001**, 46, (2), 356-367.

39. Redfield, A.C., The biological control of chemical factors in the environment. American Scientist **1958**, 46, (3), 205-221.

40. Evans-White, M. A.; Haggard, B. E.; Scott, J. T., A Review of stream nutrient criteria development in the United States. Journal of Environmental Quality **2013**, 42, (4), 1002-1014.

41. Sharpley, A. N.; Haggard, B. E.; Berry, L.; Brye, K.; Burke, J.; Daniels, M. B.; Gbur, E.; Glover, T.; Hays, P.; Kresse, T.; VanDevender, K. W., Nutrient concentrations in Big Creek correlate to regional watershed land use. Agricultural & Environmental Letters **2017**, 2:170027; doi:10.2134/ael2017.08.0027.

42. Miller, R. B.; Heeren, D. M.; Fox, G. A.; Halihan, T.; Storm, D. E.; Mittelstet, A. R., The hydraulic conductivity structure of gravel-dominated vadose zones within alluvial floodplains. Journal of Hydrology **2014**, 513, 229-240.

43. Miller, R. B.; Heeren, D. M.; Fox, G. A.; Halihan, T.; Storm, D. E., Heterogeneity influences on stream water-groundwater interactions in a gravel-dominated floodplain. Hydrological Sciences Journal-Journal Des Sciences Hydrologiques **2016**, 61, (4), 741-750.

44. Triska, F. J.; Duff, J. H.; Avanzino, R. J., The role of water exchange between a stream and its hyporheic zone in nitrogen cycling at the terrestrial aquatic interface. Hydrobiologia **1993**, 251, (1-3), 167-184.

45. Zarnetske, J. P.; Haggerty, R.; Wondzell, S. M.; Baker, M. A., Labile dissolved organic carbon supply limits hyporheic denitrification. Journal of Geophysical Research-Biogeosciences **2011**, 116, G04036; doi:10.1029/2011JG001730.

46. Zarnetske, J. P.; Haggerty, R.; Wondzell, S. M.; Bokil, V. A.; Gonzalez-Pinzon, R., Coupled transport and reaction kinetics control the nitrate source-sink function of hyporheic zones. Water Resources Research **2012**, 48, W11508; doi:10.1029/2012WR011894.

47. Harvey, J. W.; Bohlke, J. K.; Voytek, M. A.; Scott, D.; Tobias, C. R., Hyporheic zone denitrification: Controls on effective reaction depth and contribution to whole-stream mass balance. Water Resources Research **2013**, 49, (10), 6298-6316.

48. Moatar, F.; Abbott, B.W.; Minaudo, C.; Curie, F.; Pinay, G., Elemental properties, hydrology, and biology interact to shape concentration discharge curves for carbon, nutrients, sediment, and major ions. Water Resources Research **2017**, 52, (2), 1270-1287.

49. Zarnetske, J. P.; Haggerty, R.; Wondzell, S. M.; Baker, M. A., Dynamics of nitrate production and removal as a function of residence time in the hyporheic zone. Journal of Geophysical Research-Biogeosciences **2011**, 116, G01025; doi:10.1029/2010JG001356.

50. Zarnetske, J. P.; Haggerty, R.; Wondzell, S. M., Coupling multiscale observations to evaluate hyporheic nitrate removal at the reach scale. Freshwater Science **2015**, 34, (1), 172-186.

51. Palmer-Felgate, E. J.; Mortimer, R. J. G.; Krom, M. D.; Jarvie, H. P., Impact of point-source pollution on phosphorus and nitrogen cycling in stream-bed sediments. Environmental Science & Technology **2010**, 44, (3), 908-914.

52. Aubert, A. H.; Breuer, L., New seasonal shift in in-stream diurnal nitrate cycles identified by mining high-frequency data. Plos One **2016**, 11, (4)); https://doi.org/10.1371/journal.pone.0153138.

53. Dodds, W. K.; Marti, E.; Tank, J. L.; Pontius, J.; Hamilton, S. K.; Grimm, N. B.; Bowden, W. B.; McDowell, W. H.; Peterson, B. J.; Valett, H. M.; Webster, J. R.; Gregory, S., Carbon and nitrogen stoichiometry and nitrogen cycling rates in streams. Oecologia **2004,** 140, (3), 458-467.

54. Liu, T.; Xia, X. H.; Liu, S. D.; Mou, X. L.; Qiu, Y. W., Acceleration of Denitrification in Turbid Rivers Due to Denitrification Occurring on Suspended Sediment in Oxic Waters. Environmental Science & Technology **2013**, 47, (9), 4053-4061.

55. Xia, X. H.; Jia, Z. M.; Liu, T.; Zhang, S. B.; Zhang, L. W., Coupled Nitrification-Denitrification Caused by Suspended Sediment (SPS) in Rivers: Importance of SPS Size and Composition. Environmental Science & Technology **2017**, 51, (1), 212-221

56. Jarvie, H.P.; Smith, D.R., Norton L.R.; Edwards, F.; Bowes, M.J.; King, S.M.; Scarlett P.; Davies, S.; Dils, R.; Bachiller-Jareno, N. Phosphorus and Nitrogen Limitation and Impairment of Headwater Streams Relative to Rivers in Great Britain: A National Perspective on Eutrophication. Science of the Total Environment **2018**, 621, 849-862.

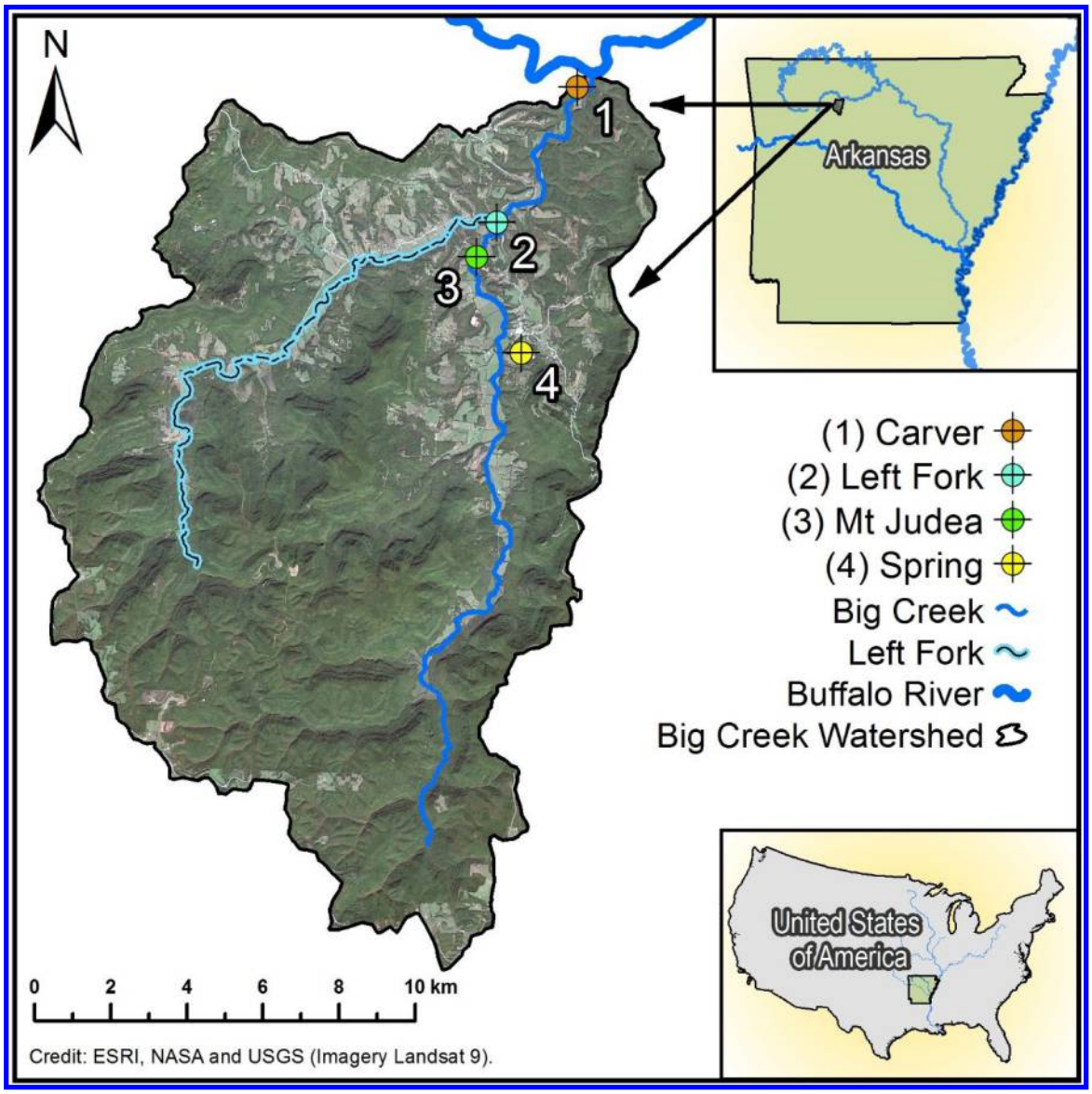

Figure 1 Map of the Big Creek watershed and its location

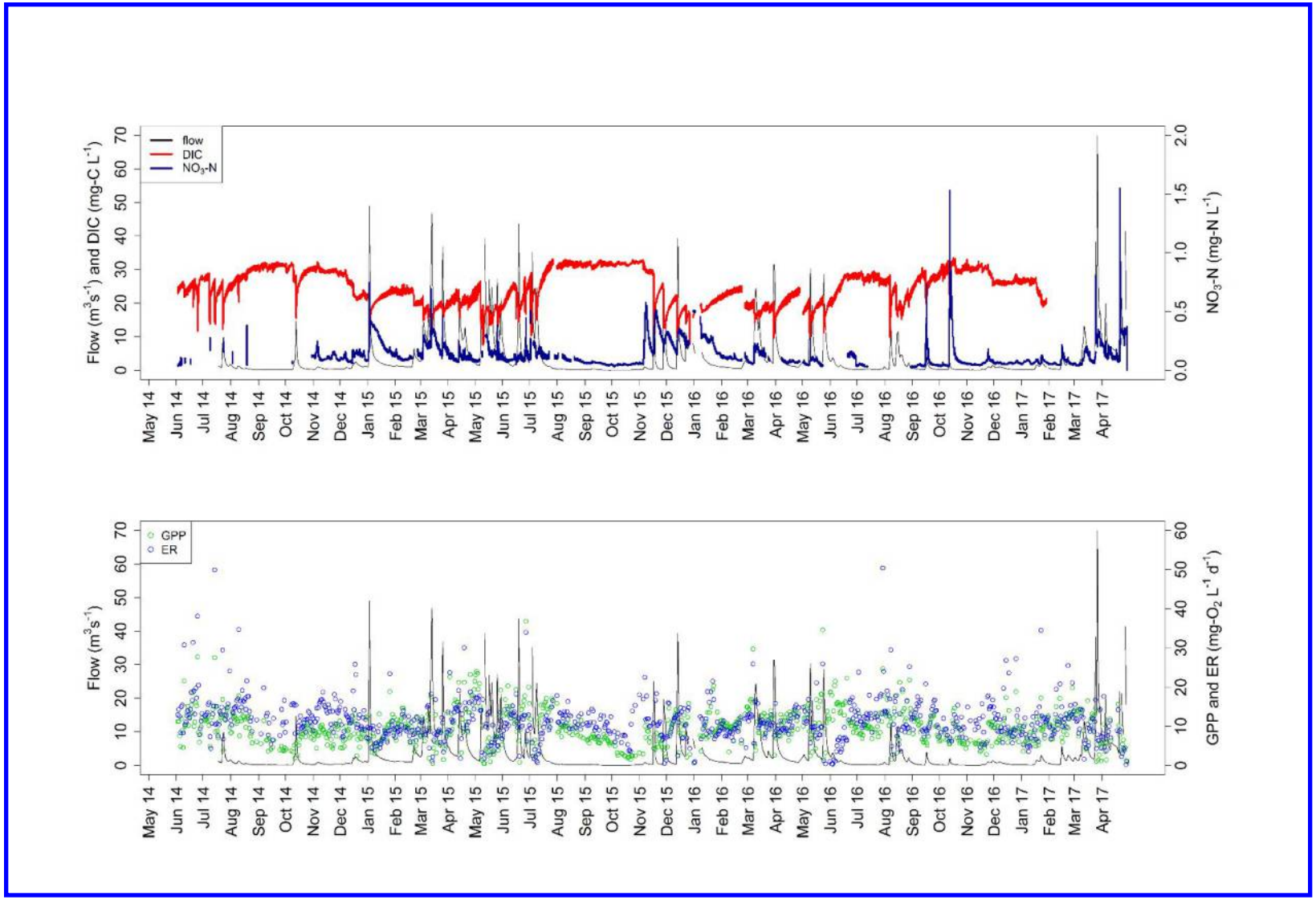

Figure 2. Time series at the downstream monitoring site (Carver), from May 2014 and May 2017, showing: (a) nitrate (NO_3-N), dissolved inorganic carbon (DIC) and stream flow; and (b) daily average gross primary production (*GPP*), ecosystem respiration (*ER*) and stream flow.

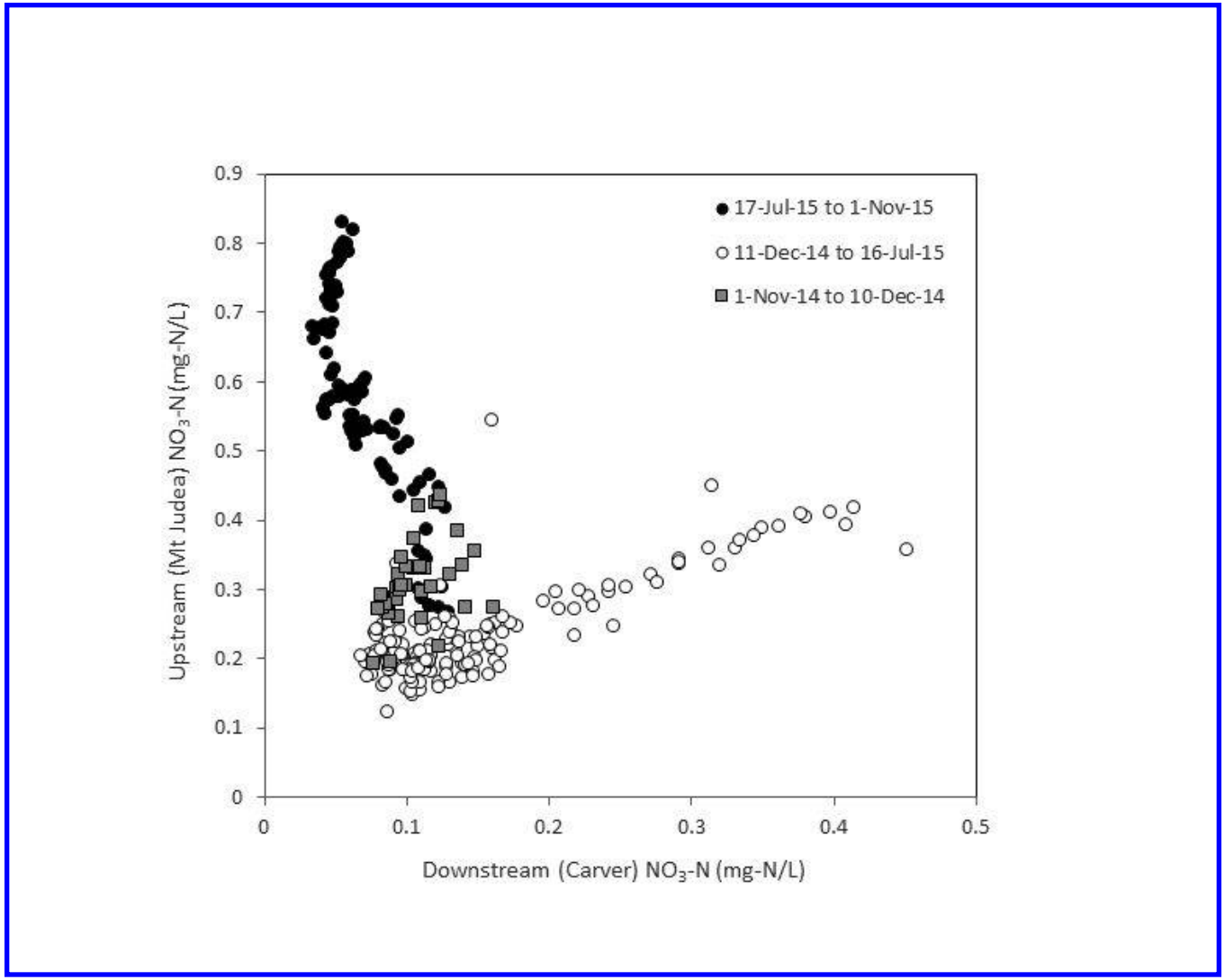

Figure 3. Scatter plot showing the relations between mean daily nitrate concentrations upstream at Mt Judea and downstream at Carver

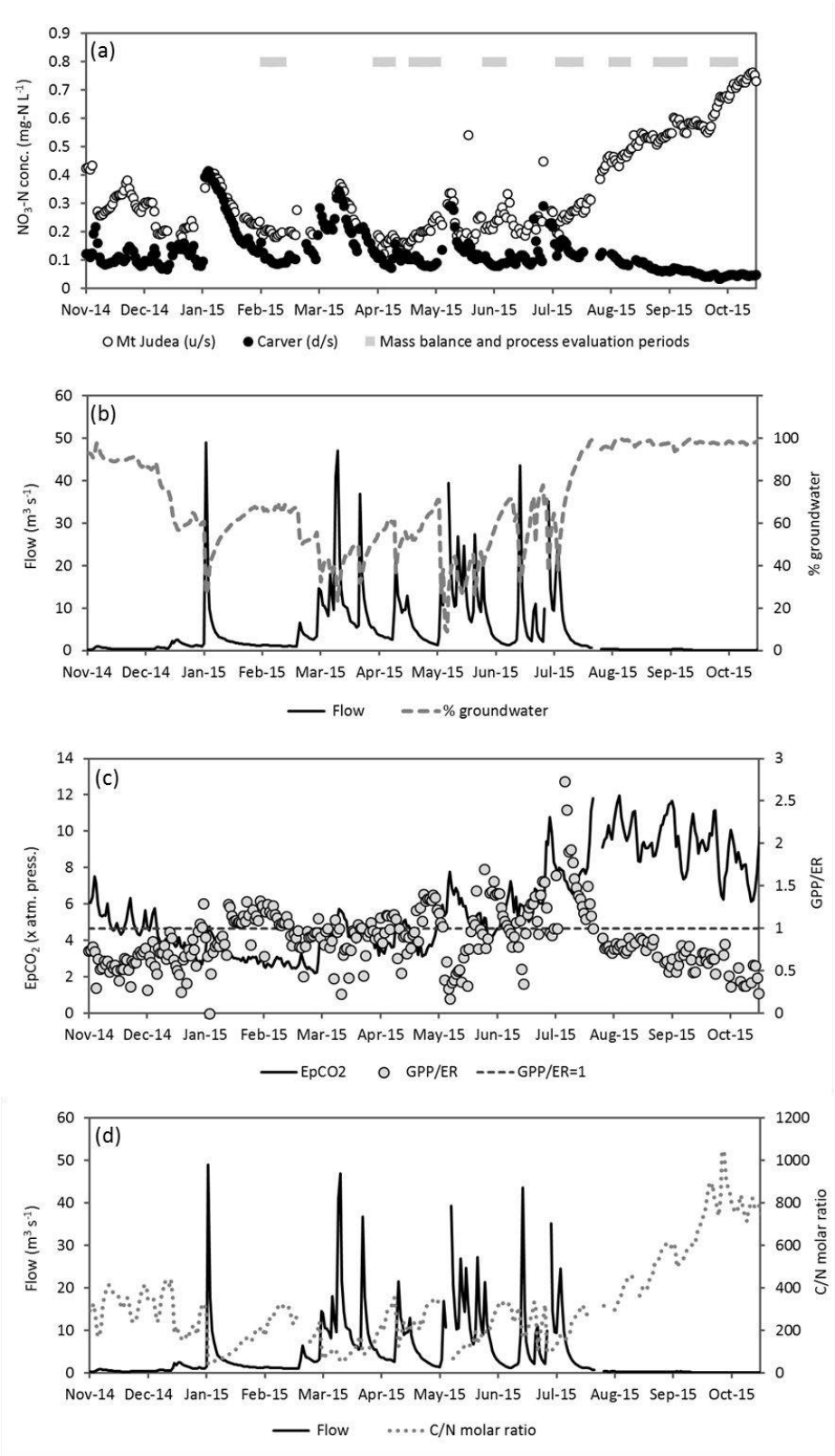

Figure 4. Time series from 1 November 2014 to 1 November 2015, showing: (a) NO_3^- concentrations upstream at Mt Judea and downstream at Carver, and the lower-flow time periods used for mass

balance calculation and evaluation of biogeochemical processes; (b) stream flow at Carver and the percentage groundwater contribution to streamflow; (c) daily ratio of gross primary production: ecosystem respiration (*GPP/ER*) (horizontal dashed line shows *GPP/ER* of 1, i.e. balance between heterotrophy and autotrophy), and excess partial pressure of carbon dioxide ($EpCO_2$); (d) streamflow and the molar C:N ratio (DIC, dissolved inorganic carbon/NO_3-N).

Season	Date range	NO_3^- input loading to reach (L_T) (kg-N d^{-1})	Instream NO_3^- removal along reach (L_R) (kg-N d^{-1})	Instream NO_3^- removal (L_R) as % of NO_3^- input loading (L_T) (U_E)
Winter	4-13 Feb 2015	17.3 (1.12)	7.68 (0.46)	44.7 (4.09)
Spring 1	5-12 Apr 2015	44.1 (6.35)	19.0 (2.82)	43.9 (9.53)
Spring 2	24 Apr - 5 May 2015	37.9 (15.3)	16.9 (3.85)	47.6 (8.93)
Early Summer	2-10 Jun 2015	49.2 (23.6)	24.1 (8.54)	51.2 (5.34)
Mid Summer	11-21 Jul 2015	61.7 (44.2)	14.6 (2.82)	32.1(14.1)
Late Summer	7-16 Aug 2015	7.56 (1.22)	5.57 (0.59)	74.2 (4.66)
Autumn 1	1-14 Sept 2015	5.81 (1.23)	4.49 (0.81)	77.8 (2.39)
Autumn 2	1-11 Oct 2015	2.98 (0.29)	2.82 (0.25)	94.8 (1.20)

Table 1: Seasonal patterns in mean daily NO_3^- input loadings (L_T) to Big Creek, mean daily instream NO_3^- load removal (L_R) along the experimental reach, under low-flow conditions, and mean daily NO_3^-load removal as a percentage of NO_3^- inputs (U_E). Standard deviations are shown in parentheses.

Season	Date range	Instream NO_3^- removal rate (U_T) (mg-N L^{-1} d^{-1})	Assimilatory NO_3^- uptake (U_A) (mg-N L^{-1} d^{-1})
Winter	4-13 Feb 2015	0.077 (0.006)	0.212 (0.035)
Spring 1	5-12 Apr 2015	0.072 (0.017)	0.256 (0.050)
Spring 2	24 Apr - 5 May 2015	0.082 (0.018)	0.355 (0.067)
Early Summer	2-10 Jun 2015	0.090 (0.014)	0.269 (0.045)
Mid Summer	11-21 Jul 2015	0.066 (0.030)	0.259 (0.040)
Late Summer	7-16 Aug 2015	0.284 (0.026)	0.180 (0.016)
Autumn 1	1-14 Sept 2015	0.229 (0.019)	0.115 (0.038)
Autumn 2	1-11 Oct 2015	0.656 (0.029)	0.076 (0.028)

Table 2: Seasonal patterns in mean daily NO_3^-removal rate (U_T) along the experimental reach of Big Creek, under low-flow conditions, and mean daily assimilatory uptake of NO_3^- by photoautotrophs (U_A). Standard deviations are shown in parentheses.

Season	Date range	Net nitrification (+) or denitrification (-) (mg-N L^{-1} d^{-1})	*GPP/ER*	$EpCO_2$ (x atm. press.)	DO (mg-O_2 L^{-1})	flow (m^3 s^{-1})	% groundwater
Winter	4-13 Feb 2015	0.135 (0.032)	1.14 (0.09)	2.80 (0.20)	11.9 (0.49)	1.15 (0.07)	66.5 (1.34)
Spring 1	5-12 Apr 2015	0.184 (0.039)	1.06 (0.13)	3.64 (0.20)	10.2 (0.33)	3.10 (0.37)	58.6 (2.38)
Spring 2	24 Apr - 5 May 2015	0.273 (0.058)	1.25 (0.16)	3.81 (0.59)	10.3 (0.50)	2.61 (1.16)	61.7 (5.79)
Early Summer	2-10 Jun 2015	0.179 (0.044)	1.34 (0.15)	4.71 (0.49)	9.39 (0.42)	3.30 (1.72)	58.0 (6.48)
Mid Summer	11-21 Jul 2015	0.193 (0.024)	1.97 (0.78)	7.15 (0.46)	8.98 (0.29)	2.54 (1.28)	82.8 (7.21)
Late Summer	7-16 Aug 2015	-0.104 (0.032)	0.78 (0.05)	10.6 (0.83)	6.95 (0.35)	0.23 (0.04)	98.8 (0.98)
Autumn 1	1-14 Sept 2015	-0.102 (0.027)	0.62 (0.10)	9.85 (1.65)	6.50 (0.54)	0.24 (0.06)	96.6 (1.42)
Autumn 2	1-11 Oct 2015	-0.592 (0.015)	0.57 (0.23)	8.17 (1.50)	7.85 (0.64)	0.04 (0.004)	97.8 (0.64)

Table 3: Seasonal patterns in mean daily NO_3^- concentration gains by net nitrification and losses by net denitrification along the experimental reach of Big Creek, under low-flow conditions, with mean daily values of the ratio between gross primary production and ecosystem respiration (*GPP/ER*), excess partial pressure of carbon dioxide ($EpCO_2$), dissolved oxygen (DO), stream flow and the percentage of groundwater contribution to stream flow. Standard deviations are shown in parentheses.

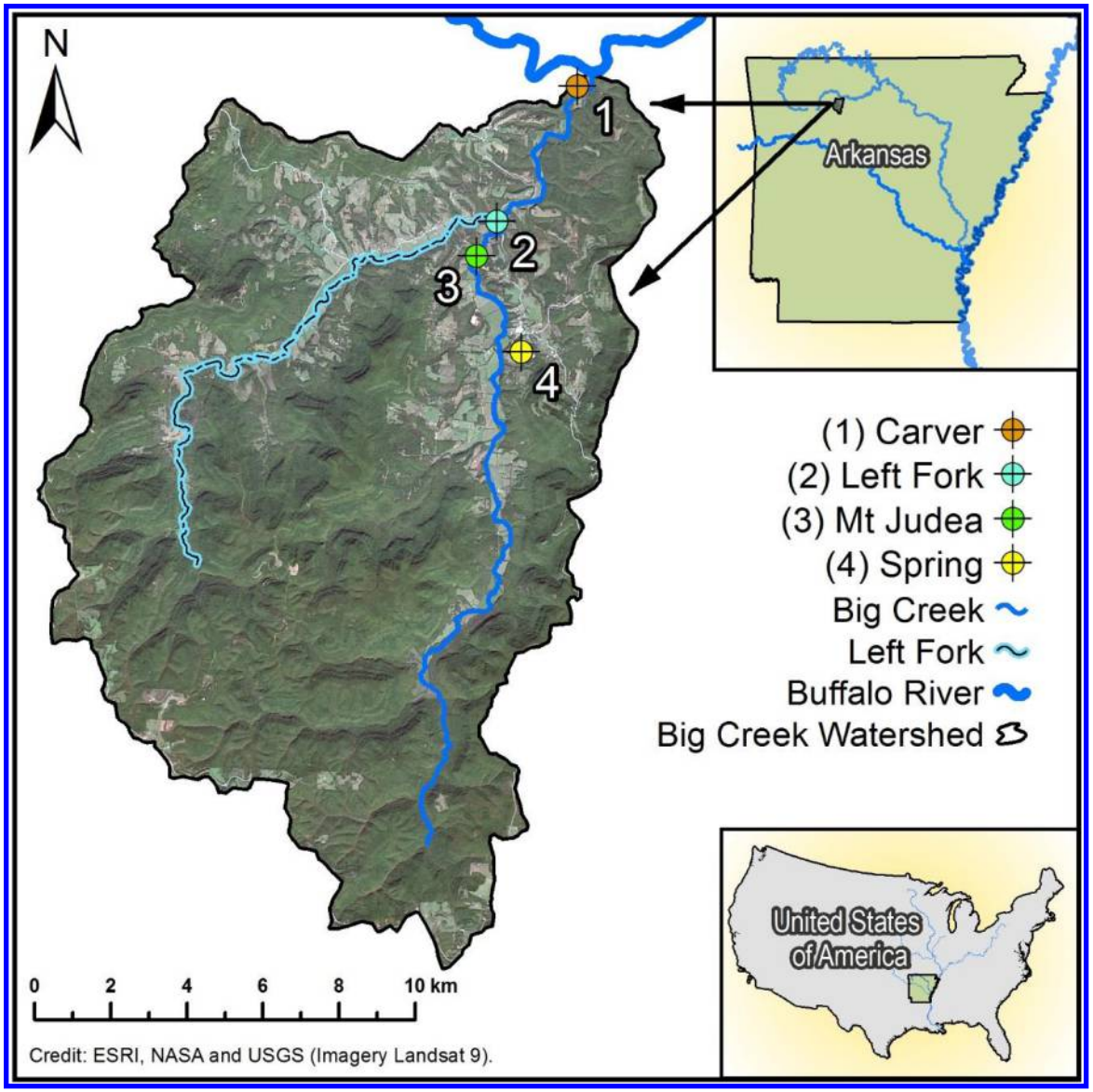
N
1
2
3
4
Arkansas
(1) Carver
(2) Left Fork
(3) Mt Judea
(4) Spring
Big Creek
Left Fork
Buffalo River
Big Creek Watershed
United States of America
0 2 4 6 8 10 km
Credit: ESRI, NASA and USGS (Imagery Landsat 9).

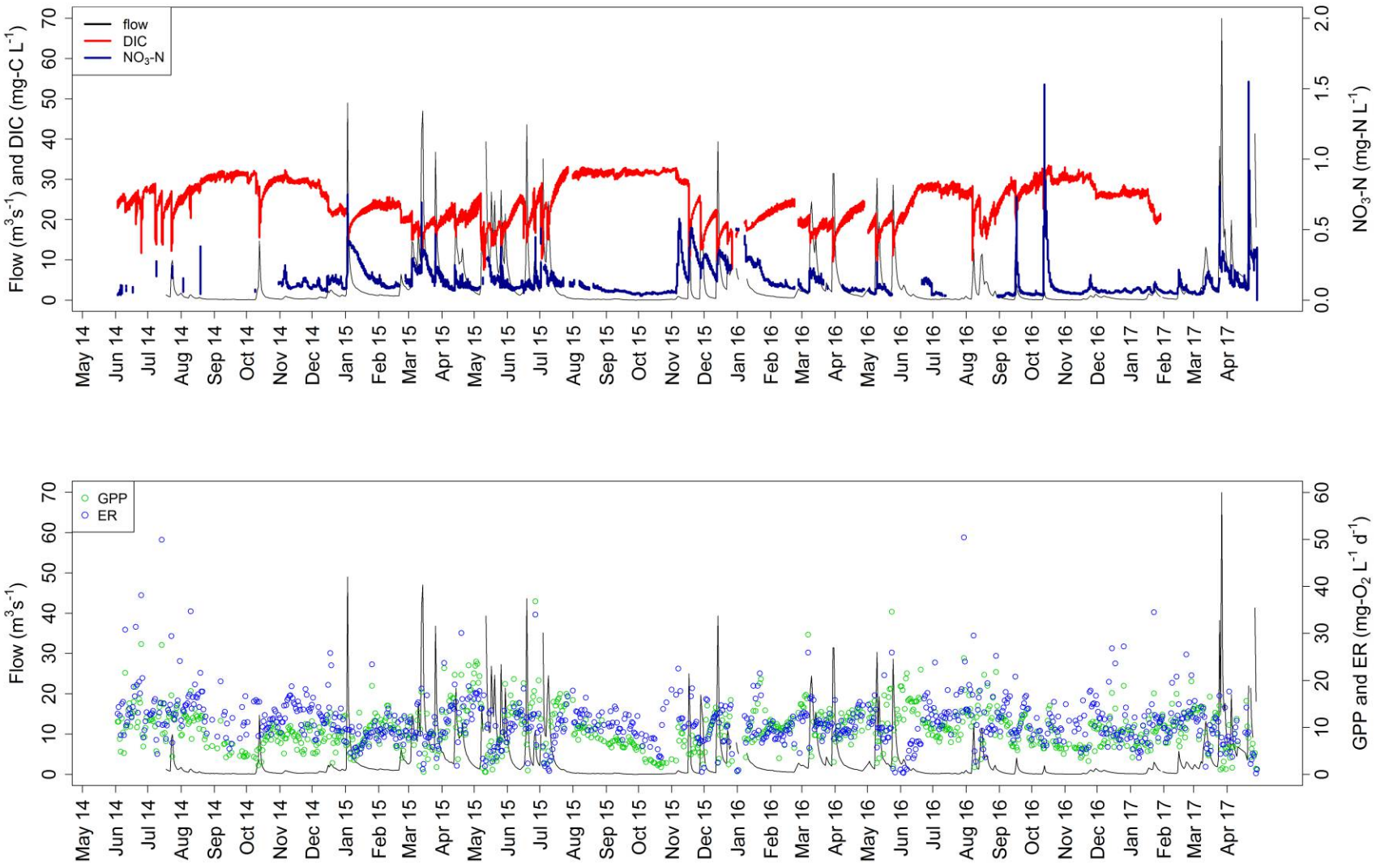
flow
DIC
NO3-N
Flow (m3s-1) and DIC (mg-C L-1)
NO3-N (mg-N L-1)
GPP
ER
Flow (m3s-1)
GPP and ER (mg-O2 L-1 d-1)
May 14
Jun 14
Jul 14
Aug 14
Sep 14
Oct 14
Nov 14
Dec 14
Jan 15
Feb 15
Mar 15
Apr 15
May 15
Jun 15
Jul 15
Aug 15
Sep 15
Oct 15
Nov 15
Dec 15
Jan 16
Feb 16
Mar 16
Apr 16
May 16
Jun 16
Jul 16
Aug 16
Sep 16
Oct 16
Nov 16
Dec 16
Jan 17
Feb 17
Mar 17
Apr 17

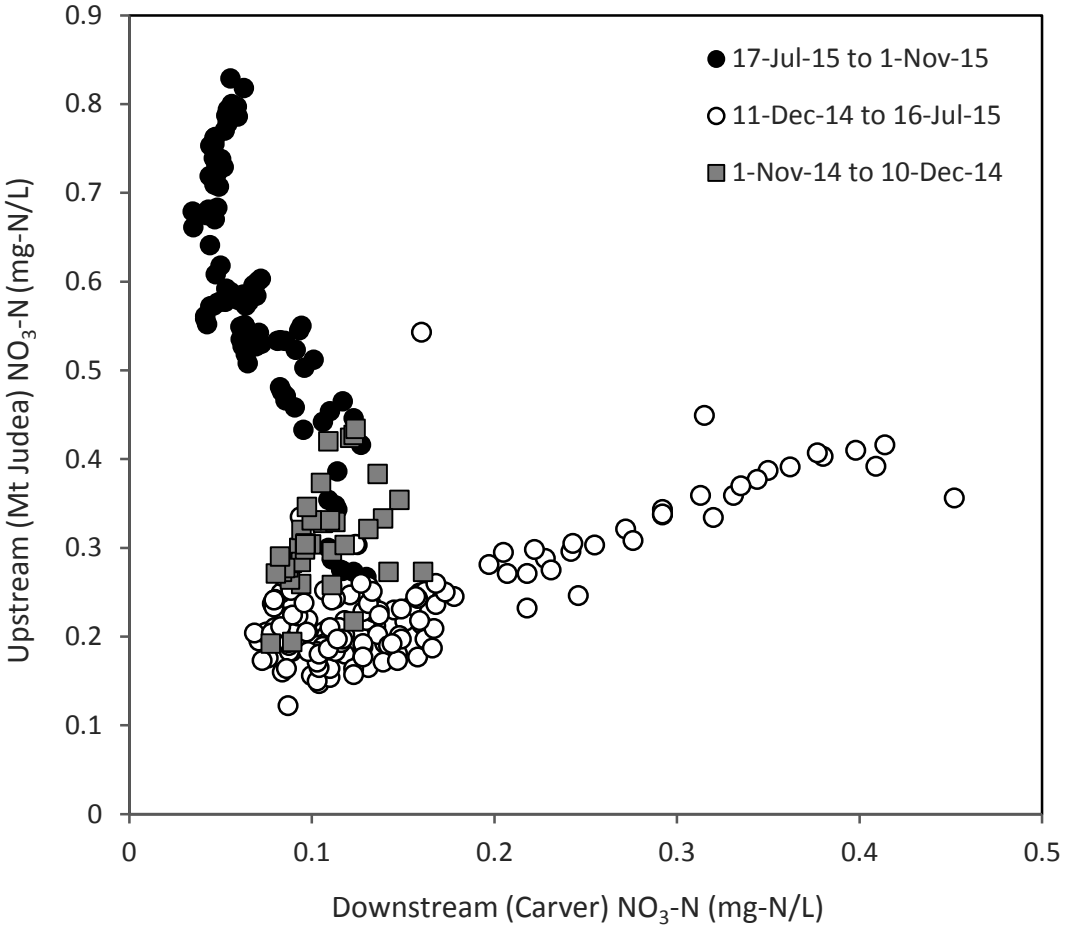
17-Jul-15 to 1-Nov-15
11-Dec-14 to 16-Jul-15
1-Nov-14 to 10-Dec-14
Upstream (Mt Judea) NO3-N (mg-N/L)
Downstream (Carver) NO3-N (mg-N/L)
0
0.1
0.2
0.3
0.4
0.5
0.6
0.7
0.8
0.9
0
0.1
0.2
0.3
0.4
0.5

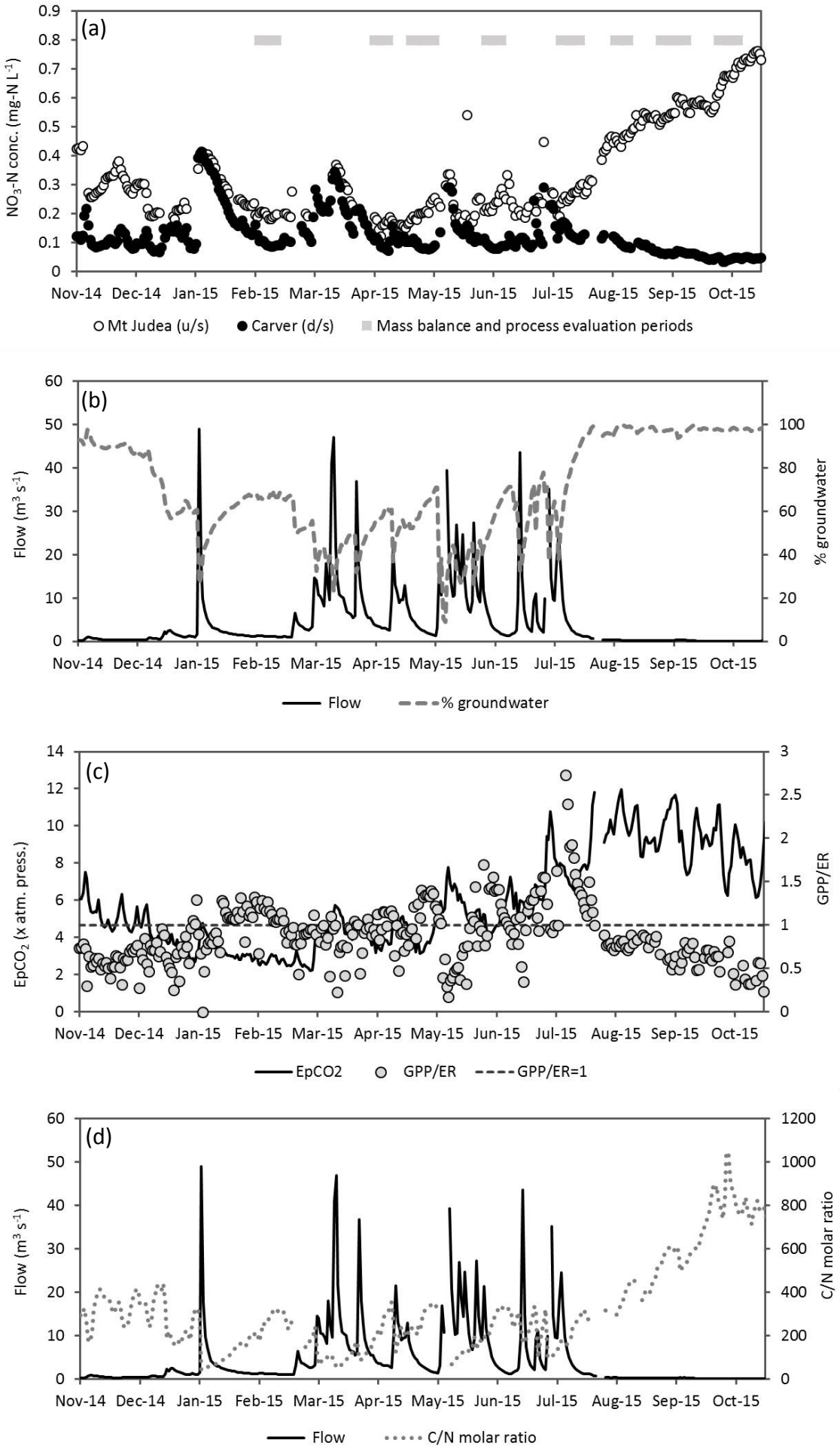
(a)
NO_3-N conc. (mg-N L^{-1})
Nov-14 Dec-14 Jan-15 Feb-15 Mar-15 Apr-15 May-15 Jun-15 Jul-15 Aug-15 Sep-15 Oct-15
Mt Judea (u/s)
Carver (d/s)
Mass balance and process evaluation periods
(b)
Flow (m^3 s^{-1})
% groundwater
Flow
% groundwater
(c)
$EpCO_2$ (x atm. press.)
GPP/ER
EpCO2
GPP/ER
GPP/ER=1
(d)
Flow (m^3 s^{-1})
C/N molar ratio
Flow
C/N molar ratio

Figure 4

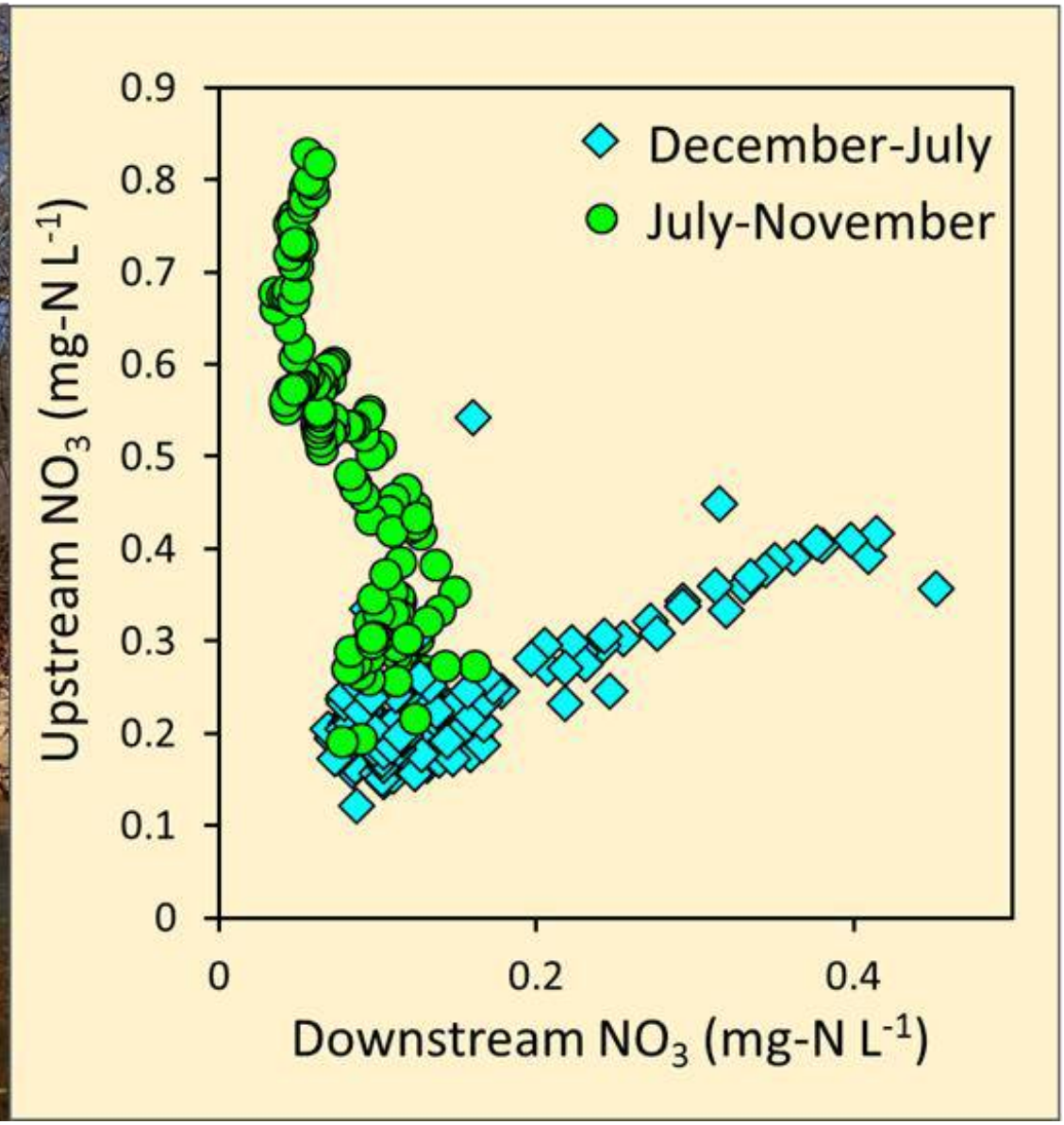
December-July
July-November
Upstream NO_3 (mg-N L^{-1})
Downstream NO_3 (mg-N L^{-1})
0
0.1
0.2
0.3
0.4
0.5
0.6
0.7
0.8
0.9
0
0.2
0.4